(NASA-TM-78454) SURFACE SHEAR STRESS MEASUREMENTS ON CIRCULAR CYLINDER IN CROSS FLOW AT NEAR-CRITICAL REYNOLDS NUMBERS (NASA) 31 p

N82-71956

Unclas
00/39 05908

NASA TM-78,454

AVAILABLE FROM ORIGINATING OFFICE ONLY

SURFACE SHEAR STRESS MEASUREMENTS ON CIRCULAR CYLINDER IN CROSS FLOW AT NEAR-CRITICAL REYNOLDS NUMBERS

V. S. Murthy and W. C. Rose

Ames Research Center
Moffett Field, Calif. 94035

REPRODUCED BY
NATIONAL TECHNICAL
INFORMATION SERVICE
U.S. DEPARTMENT OF COMMERCE
SPRINGFIELD, VA. 22161

1. Report No. NASA TM-78,454	2. Government Accession No.	3. Recipient's Catalog No.
4. Title and Subtitle SURFACE SHEAR STRESS MEASUREMENTS ON CIRCULAR CYLINDER IN CROSS FLOW AT NEAR-CRITICAL REYNOLDS NUMBERS		5. Report Date 6. Performing Organization Code
7. Author(s) V. S. Murthy* and W. C. Rose		8. Performing Organization Report No. A-7277
9. Performing Organization Name and Address NASA Ames Research Center Moffett Field, Calif. 94035		10. Work Unit No. 505-06-15 11. Contract or Grant No.
12. Sponsoring Agency Name and Address National Aeronautics and Space Administration Washington, D.C. 20546		13. Type of Report and Period Covered Technical Memorandum 14. Sponsoring Agency Code

15. Supplementary Notes

*Senior NRC Research Associate.

16. Abstract

Measurements were made of wall shear stress through the use of buried wire gages on a circular cylinder in cross flow, over the Reynolds number range of 2.7×10^5 to 7×10^6. Boundary-layer transition and separation characteristics have been determined as a function of Reynolds number. Over the mid-range of Reynolds numbers, skin friction measurements did not repeat well with different rotation angels of the cylinder, indicating possibilities of either strong three dimensionality or nonstationariness. Discrete vortex shedding seemed obvious at the lowest of the above-mentioned Reynolds numbers, but failed to become so at higher Reynolds numbers.

17. Key Words (Suggested by Author(s))	18. Distribution Statement		
Drag Separation Skin friction Boundary layers Fluid mechanics	Available from originating office only. LSTAR Category - 34		
19. Security Classif. (of this report) Unclassified	20. Security Classif. (of this page) Unclassified	21. No. of Pages 31	22. Price* $4.00

*For sale by the National Technical Information Service, Springfield, Virginia 22161

NOMENCLATURE

b	span of the sensor
C_D	drag coefficient = drag per unit span$/\frac{1}{2}\rho_\infty U_\infty^2 D$
C_f	skin friction coefficient = $\dfrac{\tau_w}{\frac{1}{2}\rho_\infty U_\infty^2}$
D	diameter of the cylinder
k	coefficient of thermal conductivity of flow medium at sensor operating temperature
k_{sub}	coefficient of thermal conductivity of substrate material
ℓ	length of sensor in flow direction
M	Mach number of the free stream
Nu	Nusselt number for the flow over the gage = $\dfrac{q - q_0}{bk(T_w - T_0)}$
Pr	molecular Prandtl number of the flow medium
p	pressure
p_∞	pressure in the undisturbed free stream
q	total heat loss from sensor in flow
q_0	heat loss from sensor in absence of any flow
Re_D	Reynolds number based on cylinder diameter = $\dfrac{\rho_\infty U_\infty D}{\mu_\infty}$
T_w	sensor temperature when heated (operating)
T_0	sensor or substrate temperature when sensor is not operating
U_∞	free-stream velocity
x	streamwise coordinate
λ	equivalent length factor of gage (determined by calibration)
μ	absolute viscosity of flow medium at sensor operating temperature
ρ	density of flow medium at sensor operating temperature and local pressure
ρ_∞	density of flow medium in undisturbed free stream
τ_w	wall shear stress

SURFACE SHEAR STRESS MEASUREMENTS ON CIRCULAR CYLINDER IN CROSS FLOW AT NEAR-CRITICAL REYNOLDS NUMBERS

V. S. Murthy* and W. C. Rose

Ames Research Center

SUMMARY

Measurements were made of wall shear stress through the use of buried wire gages on a circular cylinder in cross flow, over the Reynolds number range of 2.7×10^5 to 7×10^6. Boundary-layer transition and separation characteristics have been determined as a function of Reynolds number. Over the mid-range of Reynolds numbers, skin friction measurements did not repeat well with different rotation angles of the cylinder, indicating possibilities of either strong three dimensionality or nonstationariness. Discrete vortex shedding seemed obvious at the lowest of the above-mentioned Reynolds numbers, but failed to become so at higher Reynolds numbers.

INTRODUCTION

Circular cylinders in cross flow have remained subjects of sustained interest because of their relevance to wind effects on tall chimney-type structures, to flow past tube banks in heat exchangers, to aerodynamics of aircraft and missiles at high angles of attack, to ocean current effects on cold water pipes in Ocean Thermal Energy Conversion (OTEC) plants, etc. Across the critical range of Reynolds numbers (2×10^5 to 3×10^6), the flow pattern undergoes large changes to exhibit strong three dimensionality and significant sensitivity to surface roughness (ref. 1). Development of analytical calculational methods for this range of Reynolds numbers has met with only limited success, and any improvements in them perhaps requires additional inputs in terms of extended experimental data. Much of the experimental data that exists now is confined to measured pressure distributions, with limited information on boundary-layer growth (refs. 2-9). For Reynolds numbers above this range, there is considerable interest in terms of real life applications, but almost no experimental or theoretical data (refs. 4,6). Existing test facilities cannot directly offer Reynolds numbers much higher than 6×10^6, while the theoretical methods must await validation through comparisons with at least some experimental data before their predictions could be fully relied on. A more detailed verification with experimental data, than simply the pressure distributions and gross features of flow separation, might help establish greater reliance on theoretical predictions. If this were achieved even at the experimentally accessible Reynolds number

*Senior NRC Research Associate.

range, it would still provide a much firmer base than exists now for projecting the theoretical methods beyond those Reynolds number limits. Verifications of this kind are possible if, for example, the boundary-layer details are measured.

The measurements reported here were part of a larger test series and consisted of determining the skin friction (surface shear stress) distributions for subsonic cross flow past a circular cylinder at different Reynolds numbers. A relatively new technique that employs buried wire gages (ref. 10) was used to measure skin friction.

EXPERIMENT

Present data were acquired in two different wind tunnels. One is the variable density, low-turbulence (less than 0.25%), 366-cm (12-ft) diam pressure tunnel at NASA Ames Research Center, Moffett Field, California. The other is the GALCIT low-turbulence (about 0.5%), 306-cm (10-ft) diam tunnel at the Graduate Aeronautical Laboratories, California Institute of Technology, Pasadena, California. The model used was a 30.48-cm diam, 259-cm long, hollow circular cylinder equipped with conventional surface pressure taps and some specially developed buried wire gages (ref. 10) that allowed measurement of wall shear stress (see figs. 1,2). This latter technique of measuring wall shear stress with buried wire gages and others of that kind had its origin long ago (ref. 11), but started becoming popular only recently when special methods were developed for fabricating durable and reliable gages (refs. 10,12). A brief description of this technique is given here to reduce the dependence of this presentation on other references (refs. 10,13).

The Buried Wire Gage Technique

The buried wire gage consists of a slender wire extending between two flush embedded electrical leads on a low thermal conductivity substrate surface and remaining well-attached throughout its span to the surface. The wire is electrically heated to a constant temperature from an anemometer system and the heat loss from it to the flow is converted to skin friction through a predetermined calibration which follows the law (ref. 13),

$$\frac{\rho \tau_w (\lambda \ell)^2 Pr}{\mu^2} = 1.9\ Nu^3 - 0.2778\ \frac{\rho (\lambda \ell)^3 Pr}{\mu^2}\ \frac{dp}{dx}\ \frac{1}{Nu} \tag{1}$$

with

$$Nu = \frac{q - q_0}{bk(T_w - T_0)}$$

The quantities q_0 and λ are calibration constants which may respectively be determined by two simple measurements, one in the absence of any

flow and the other in a flow with known skin friction. For a thin wire, the term involving pressure gradient becomes very small compared to the other terms and may simply be ignored in most practical situations. In addition to this important feature, this technique exhibits several other advantages. The gages are nonintrusive to flow and hence may be arranged at a large number of streamwise stations for simultaneous use. They are relatively easy to arrange on wind-tunnel models and achieve calibrations that remain unaltered over changes in boundary-layer status, laminar or turbulent.

In the present test series, gages were arranged on five plugs (see fig. 1) which could be mounted flush to the cylinder surface. Two different configurations of gages were used, single wire gages and triple wire gages. The single wire gages were primarily used for measuring skin friction, whereas the triple wire gages were further used for cross correlation of adjacent wire signals. Calibrations of some gages were achieved by performing heat transfer measurements in still air, and by comparing, for a relatively low Reynolds number flow past the cylinder, a measurement at one angular location with analytically computed (ref. 14) skin friction for that angular location. This approach was used only for those gages that could be positioned in the laminar part of the boundary layer upon which the theoretical calculations can be fully relied. Other gages that could not be positioned in this manner because of restrictions imposed by model installation were calibrated by again making one measurement at still air conditions and one measurement with the flow conditions and angular location identical to that of a previous measurement using one of the calibrated gages.

Test Program

All the gages used in this test series were of the solvent buried type (ref. 10) with 5-μm diam tungsten wires as sensors and polystyrene as substrate material (see fig. 2). The gages were operated in a constant temperature mode with sensor temperatures maintained around a relatively low value of about 60° C, so that the substrate material could remain below its softening point. Square wave tests revealed that the gages, because of the associated long cables, exhibited an upper frequency limit of only 20 kHz. The test series covered a Reynolds number (based on cylinder diameter) range of 2×10^5 to 7×10^6. Both pressures and skin friction were measured at 2° angular intervals.

RESULTS AND DISCUSSION

The results of measurements are seen plotted in figures 3 to 9. Different symbols in skin friction plots denote different gages. At the lowest Reynolds number of 2.7×10^5 (see fig. 3), the boundary layer appears to stay laminar all the way to the separation point. The measured skin friction distribution identifies the separation point very clearly.

At the next higher Reynolds number of 0.84×10^6 (see fig. 4), the boundary layer appears to stay laminar up to the angle of 80°, above which there is evidence of transition to turbulent state. Some of the measured skin friction values in the angle range of 80° to 120° are very large, indicating the possibility of a turbulent boundary layer in this region. The measurements of different gages do not, however, show continuity in this angular range and suggest that the flow is either strongly three dimensional or nonstationary with the cylinder rotation angle or both. The present investigation was not equipped to explore this question any further. Flow separation seems to have been accompanied by reattachment and final separation. A very similar behavior seems to occur at the next two higher Reynolds numbers of 1.7×10^6 and 2.5×10^6 (see figs. 5, 6). Evidence of three dimensionality is seen even at lower angles. In all the above cases, the measured mean pressure distributions do not seem to provide any immediately obvious evidence of three dimensionality.

Skin friction distributions for the next three higher Reynolds numbers of 3.5×10^6, 5×10^6, and 7×10^6 (see figs. 7, 8, 9) do not show any evidence of reattachment. Transition to turbulent boundary layer seems to be well defined by the relatively abrupt increases in skin friction.

Measurements at the lowest Reynolds number are compared in figures 10 and 11 with earlier measurements by other investigators. There is generally good agreement between the different skin friction data, especially at the lower angles and at the separation point. The differences that prevail over the middle range of angles could be attributed to two different factors. One is the effect of wind-tunnel blockage which is different in different cases. This effect is even evident in the measured pressure distributions (fig. 11). The other factor is the possible inadequacy in the definition of normalized skin friction coefficient (fig. 10). Because of the effects of streamwise pressure gradients which are different for different sizes of cylinders, the skin friction coefficient may not be adequately scaled by the square root of Reynolds number. As of now, there is no simple scheme by which the above factors can be accounted.

Similar comparisons at slightly higher Reynolds number are shown in figures 12 and 13. These figures also contain, for quick reference, part of the comparison for the lower Reynolds number already shown in figures 10 and 11. Apart from the commonality of the reattachment phenomena, agreement at the higher Reynolds number is not as good as that at lower Reynolds number. The lack of good agreement is seen in both skin friction and pressure distributions. Present skin friction measurements show the separation, reattachment, and final separation points to be forward of those detected in Achenbach's (ref. 2) measurements. This should perhaps have been expected because wind-tunnel blockage for Achenbach's measurements (15-cm diam cylinder in 90-cm tunnel height) is higher than the blockage in present measurements (30.48-cm diam cylinder in 366-cm diam test section) and, therefore, provides an increased favorable pressure gradient ahead of the separation point, as seen in figure 13. In terms of actual skin friction values, present measurements show higher values than Achenbach's measurements. Differences of this nature

between present measurements and Achenbach's measurements prevail even at other higher Reynolds numbers.

Signals of adjacent gages could be correlated to better define the local flow direction and from that, the separation point. Figure 14 presents, for the Reynolds number of 7×10^6, a series of oscilloscope traces that represent cross correlations between two adjacent gage signals as the gages were rotated to increasing angular positions. In the present arrangement, the zero delay line has been adjusted to the middle line of the trace and a correlation peak anywhere on the right side of the middle line would imply a local streamwise flow in the direction of increasing angles. It is seen from the traces that a movement of the forward gage from 96° position to 98° position causes the correlation peak to shift from a rightward position to the middle line, implying the presence of a separation point at the gages. Correlations of this type have been obtained at other Reynolds numbers, with less success over the middle range of 0.84×10^6 to 2.5×10^6, where the indications were not as strong.

The gage systems were capable of responding to an upper frequency limit of about 20 kHz and, therefore, could be used for determining dominant frequencies in the flow. The signals were processed in a frequency analyzer to obtain frequency spectra, a few of which are displayed in figure 15. Any dominant discrete frequency in such spectra would be the vortex shedding frequency for that flow condition. Such a discrete shedding frequency could be found only at the lowest Reynolds number of 2.7×10^5, as shown on the left side of figure 15. At other higher Reynolds numbers in the range 5×10^5 to 3×10^6, the spectra failed to show discrete peaks consistently for all the angular positions of the cylinder, as typically represented by the two cases shown on the right side of figure 15. Peaks appearing at one rotational position did not necessarily appear at all other rotations. Peaks, when they appeared, corresponded to a Strouhal number (= shedding frequency × cylinder diameter/free-stream velocity) of about 0.2. For Reynolds numbers higher than 3×10^6, the spectra showed no peaks, but only a distributed energy content in a frequency range that corresponded to a Strouhal number range of 0 to 0.4.

The high frequency response of the gages made it possible to confirm the location of boundary-layer transition, already indicated by an abrupt increase in the measured skin friction values. Root mean square values of the fluctuating components of gage signals were found to show localized peaks at transition points. The peaks were quite sharp in most cases, except in the Reynolds number range of 5×10^5 to 3×10^6.

The findings on separation phenomena and or boundary-layer transition are summarized in figure 16. For Reynolds numbers up to 5×10^5, the boundary layer stays laminar all the way until separation at about 72°. In the next Reynolds number range of 5×10^5 to 3×10^6, the flow seems to become strongly three dimensional, with boundary-layer transition followed by separation, reattachment and final separation. Beyond the Reynolds number of 3×10^6, boundary-layer transition seems to move further forward on the cylinder, with separation following at about 96°.

Additional measurements performed in the GALCIT tunnel are shown in figure 17. These included some measurements with surface roughness in the form of 40% open square mesh screens wrapped around the cylinder. The screen had 0.0165-cm diam wires overlapping in the mesh and therefore was taken to represent a roughness height of two wire diameters, namely 0.033 cm. Appropriate cutouts were made in the screen to expose the gage faces to flow. Reynolds number for these measurements was 1.2×10^6, which is in the range where strong three dimensionality prevails for smooth cylinders. Skin friction measurements of the two gages superpose (see fig. 17) quite well for the smooth cylinder case to show existence of reattachment and final separation beyond the initial separation point. For the case with roughness, however, the gage data did not superpose well, but did indicate higher skin friction values with no evidence of reattachment phenomenon. Comparisons of these measurements with Achenbach's data are shown in figures 18 and 19. There is generally good agreement in terms of separation points, but not in terms of skin friction values. Present measurements indicate much higher skin friction values. Firm conclusions about the actual skin friction values for the case with roughness cannot be drawn at this stage because of the disagreement between measurements of the two different gages.

CONCLUSIONS

Skin friction distributions were measured using buried wire gages for flow past circular cylinder in the Reynolds number range of 2×10^5 to 7×10^6. These distributions were able to clearly indicate boundary-layer transition and separation phenomena. It was concluded that the Reynolds number range of 5×10^5 to 3×10^6 is characterized by strong three-dimensional effects and by reattachment phenomenon. Comparisons of measured skin friction distributions with earlier measurements by other investigators show good agreement at low Reynolds numbers. Discrete vortex shedding could be detected at low Reynolds numbers, but was not that obvious at higher Reynolds numbers in the range 5×10^5 to 3×10^6, where the shedding phenomenon seemed to change with cylinder rotation. At Reynolds numbers above 3×10^6, the shedding was characterized by a wide band frequency spectrum.

REFERENCES

1. Markovin, M. V.: Flow Around Circular Cylinder — A Kaleidoscope of Challenging Fluid Penomena. Symposium on Fully Separated Flows, Arthur G. Hansen, ed., Amer. Soc. of Mech. Eng., May 18-20, 1964, pp. 102-118.

2. Achenbach, E.: Distribution of Local Pressure and Skin Friction Around a Circular Cylinder in Cross Flow up to Re = 5×10^6. J. Fluid Mech., vol. 34, part 4, 1968, pp. 625-639.

3. Achenbach, E.: Influence of Surface Roughness on the Cross Flow Around a Circular Cylinder. J. Fluid Mech., vol. 46, part 2, 1971, pp. 321-335.

4. Roshko, A.: Experiments on the Flow Past a Circular Cylinder at Very High Reynolds Numbers. J. Fluid Mech., vol. 10, 1961, pp. 345-356.

5. Schmidt, L. V.: Measurements of Fluctuating Air Loads on a Circular Cylinder. J. Aircraft, vol. 2, no. 1, Jan.-Feb. 1965, pp. 49-65.

6. Szechenyi, E.: Supercritical Reynolds Number Simulation for Two-Dimensional Flow over Circular Cylinders. J. Fluid Mech., vol. 70, part 3, 1975, pp. 529-542.

7. Jorgensen, L. H.: Estimation of Aerodynamics for Slender Bodies Alone and With Lifting Surfaces at α's from 0° to 90°. AIAA J., vol. 11, no. 3, March 1973, pp. 409-412.

8. Macha, J. M.: A Wind Tunnel Investigation of Circular and Straked Cylinders in Transonic Cross Flow. TAMU Rep. 3319-76-01, Texas A&M Res. Found., College Station, Tex., Nov. 1976.

9. Jorgensen, L. H.: Prediction of Static Aerodynamic Characteristics for Space-Shuttle-Like and Other Bodies at Angles of Attack from 0° to 180°. NASA TN D-6996, 1973.

10. Murthy, V. S.; and Rose, W. C.: Form Drag, Skin Friction and Vortex Shedding Frequencies for Subsonic and Transonic Cross Flows on Circular Cylinder. AIAA Paper 77-687, Albuquerque, New Mex., June 27-29, 1977.

11. Liepmann, H. W.; and Skinner, G. T.: Shearing Stress Measurements by Use of a Heated Element. NACA TN-3268, 1954.

12. Rubesin, M. W.; Okuno, A. F.; Mateer, G. G.; and Brosh, A.: A Hot Wire Surface Gage for Skin Friction and Separation Detection Measurements. NASA TM X-62,465, 1975.

13. Brown, G. L.: Theory and Application of Heated Films for Skin Friction Measurements. Proceedings of the 1967 Heat Transfer and Fluid Mechanics Institute. Stanford Univ. Press, Stanford, Calif., pp. 361-381.

14. Murphy, J. D.; and Davis, C. B.: User's Guide — Ames Inlet Boundary Layer Program MK-I. NASA TM X-62,211, 1973.

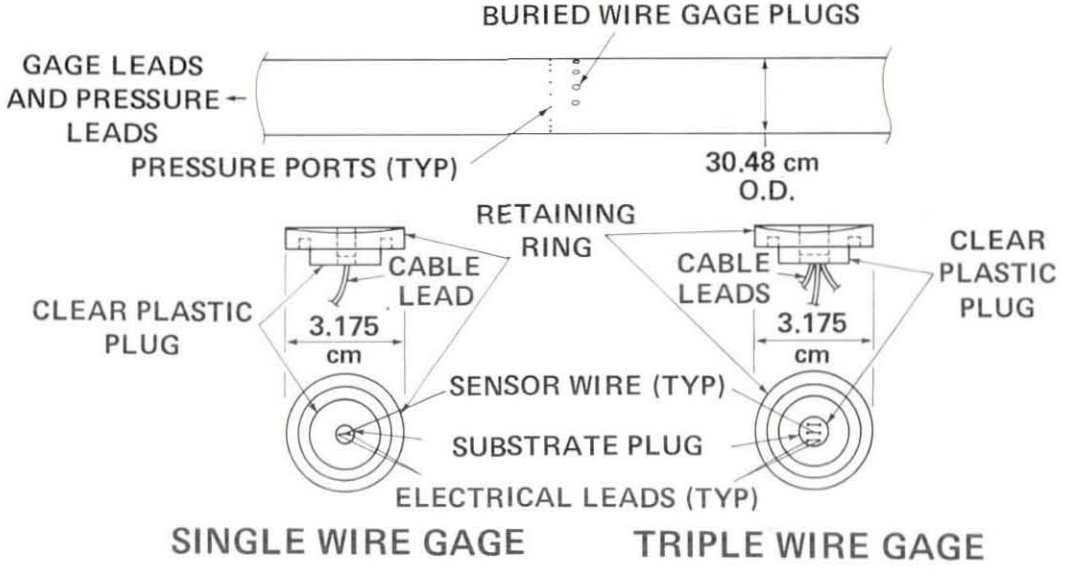

Figure 1.- Schematic of model and buried wire gages.

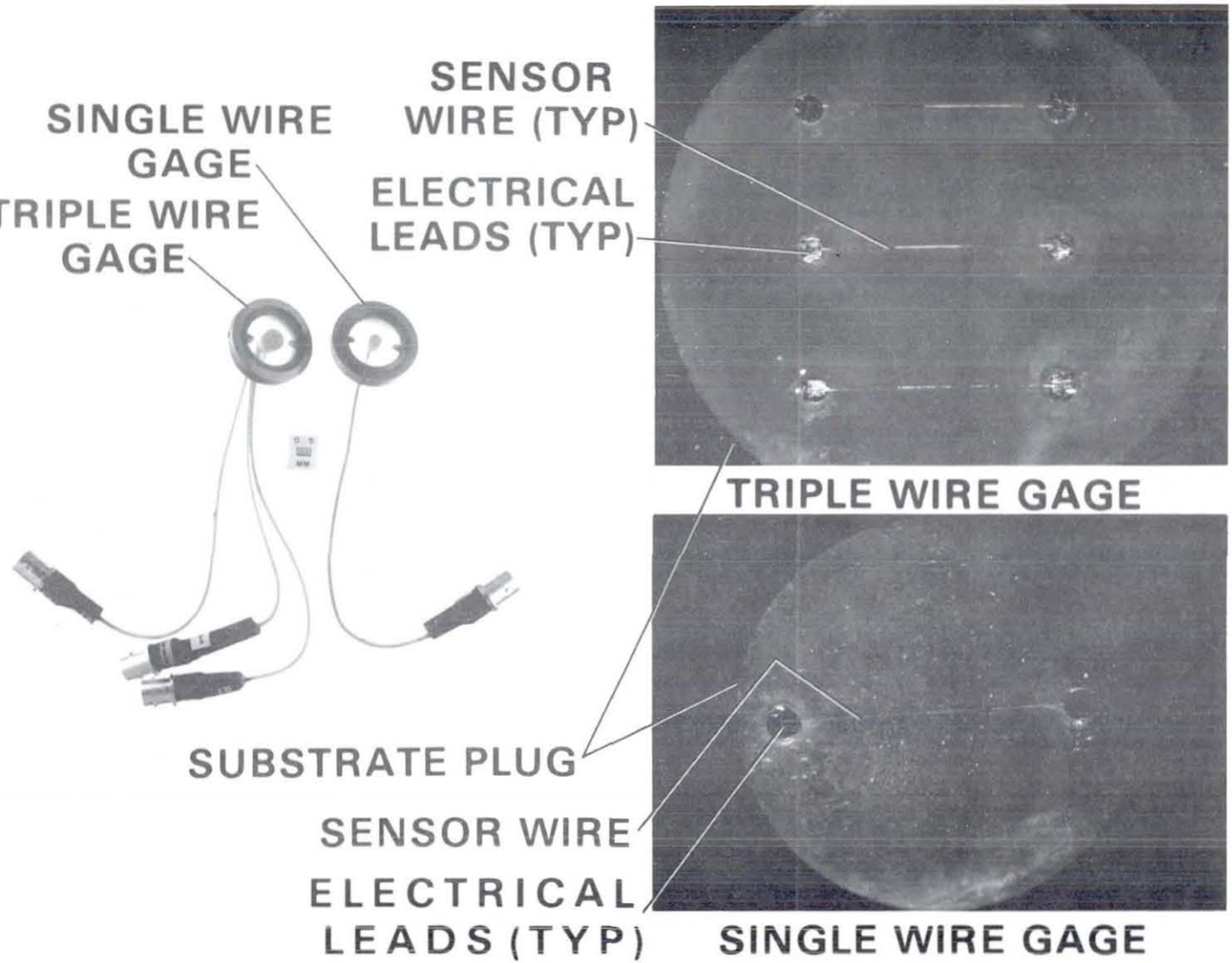

Figure 2.- Photographs of buried-wire gages.

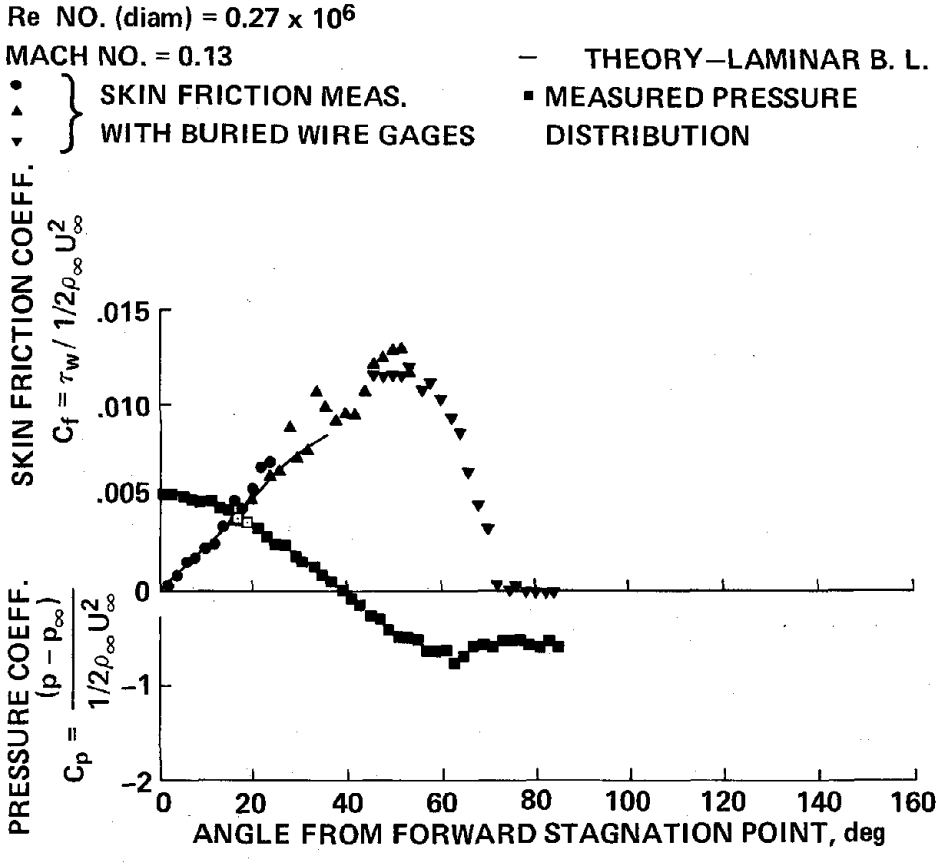

Figure 3.- Skin friction and pressure distributions on circular cylinder.

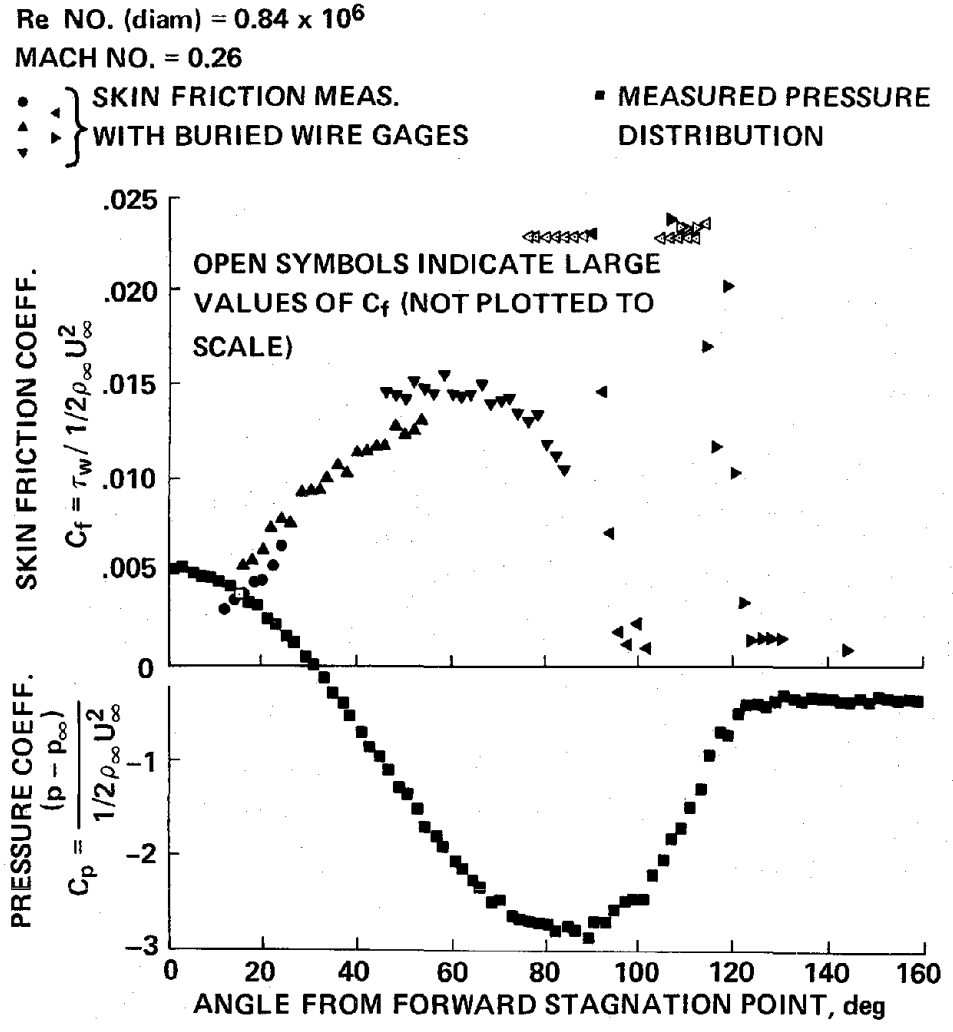

Figure 4.- Skin friction and pressure distributions on circular cylinder.

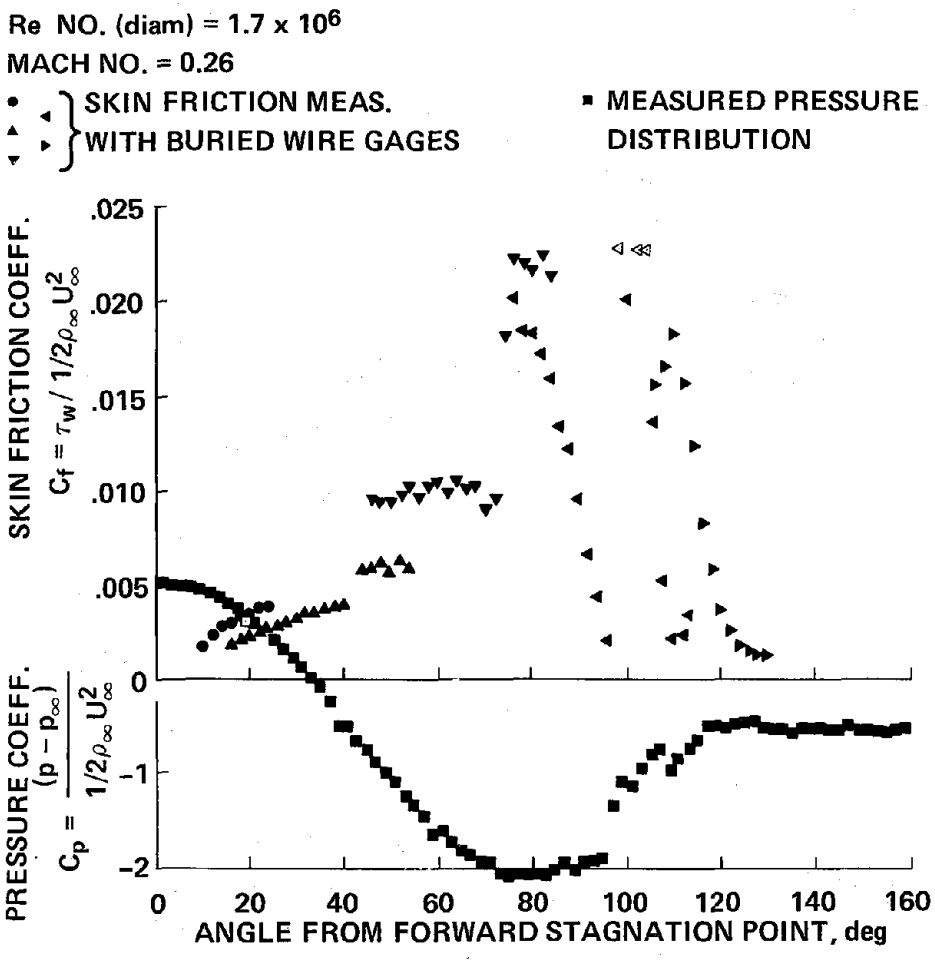

Figure 5.- Skin friction and pressure distributions on circular cylinder.

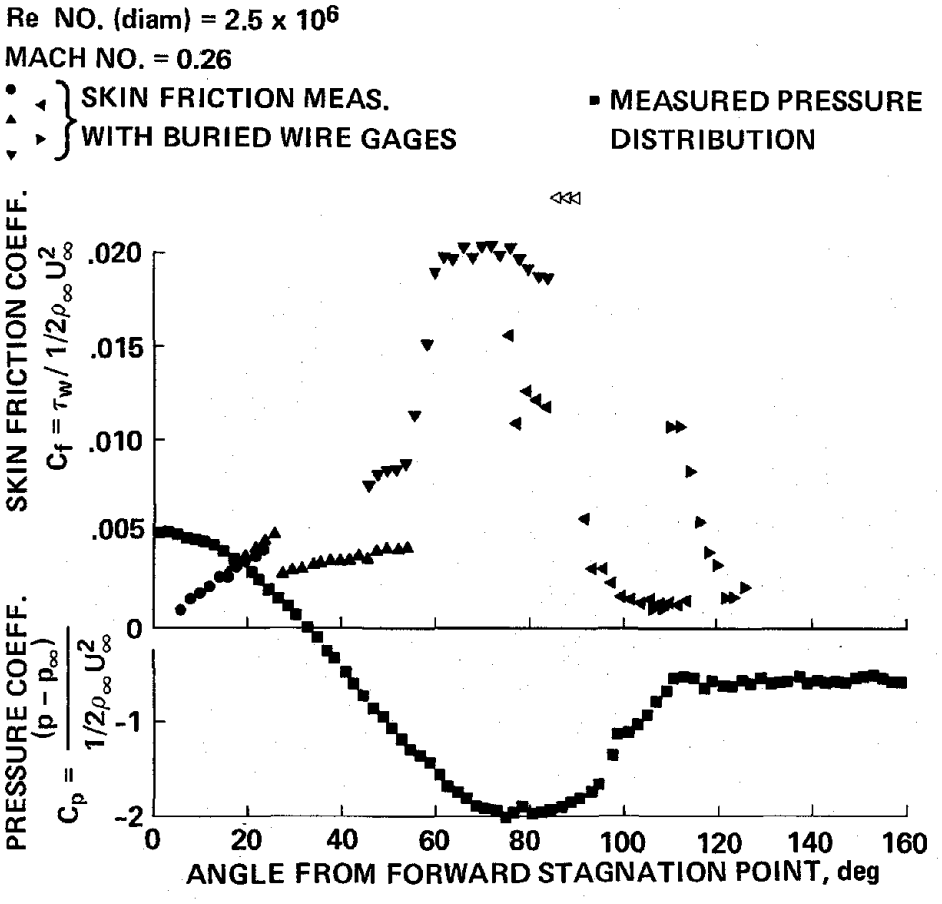

Figure 6.- Skin friction and pressure distributions on circular cylinder.

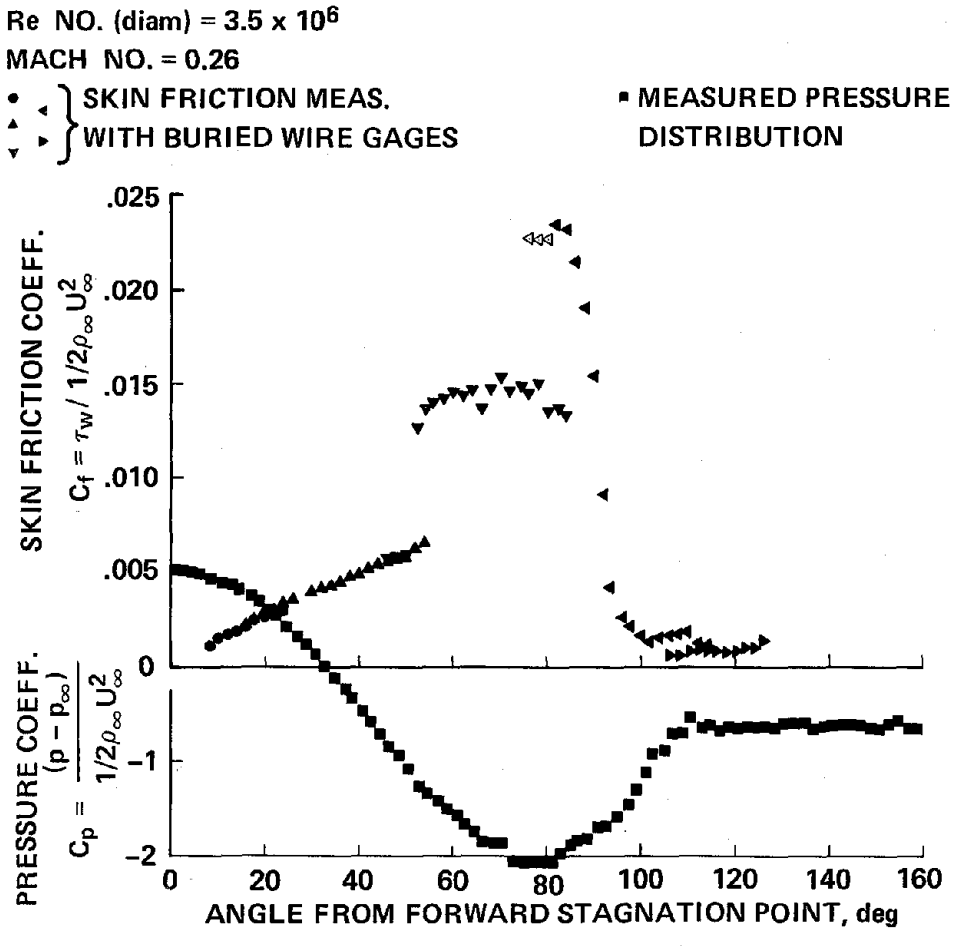

Figure 7.- Skin friction and pressure distributions on circular cylinder.

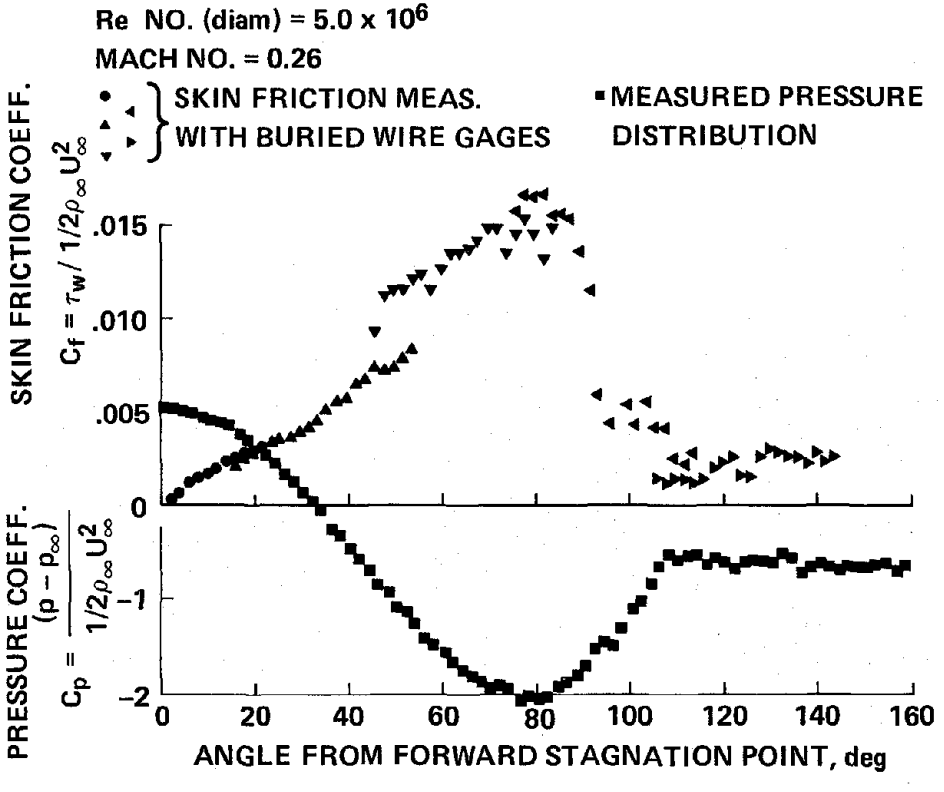

Figure 8.- Skin friction and pressure distributions on circular cylinder.

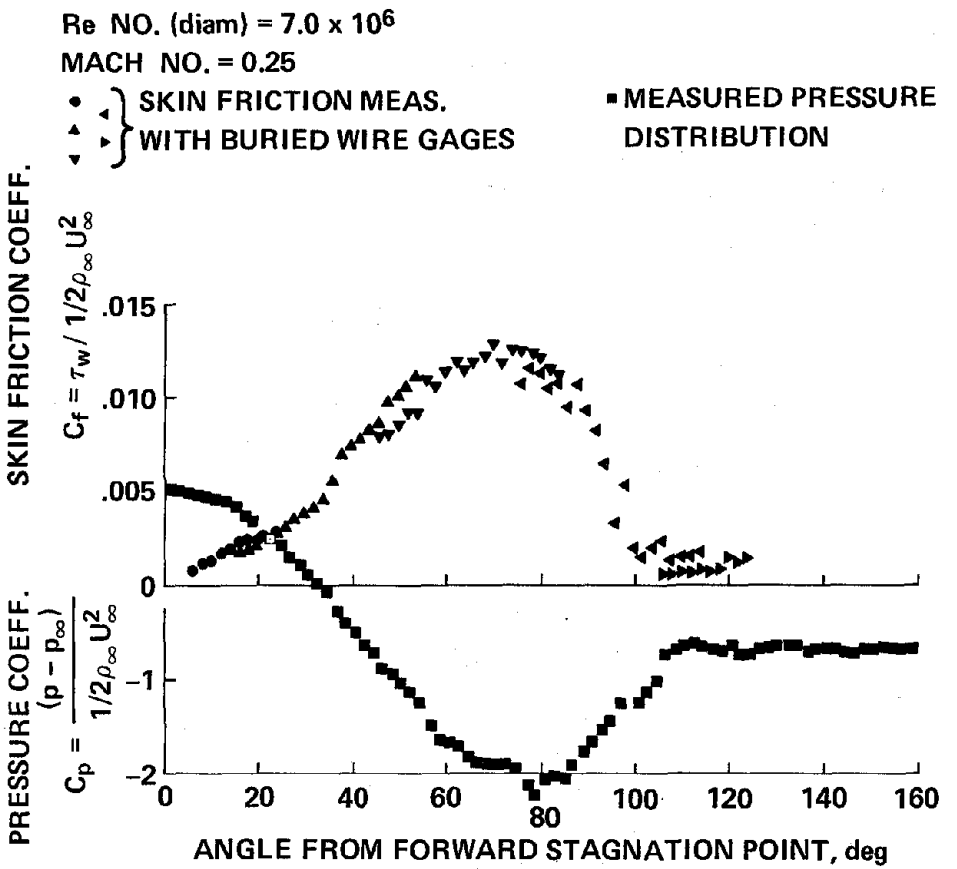

Figure 9.- Skin friction and pressure distributions on circular cylinder.

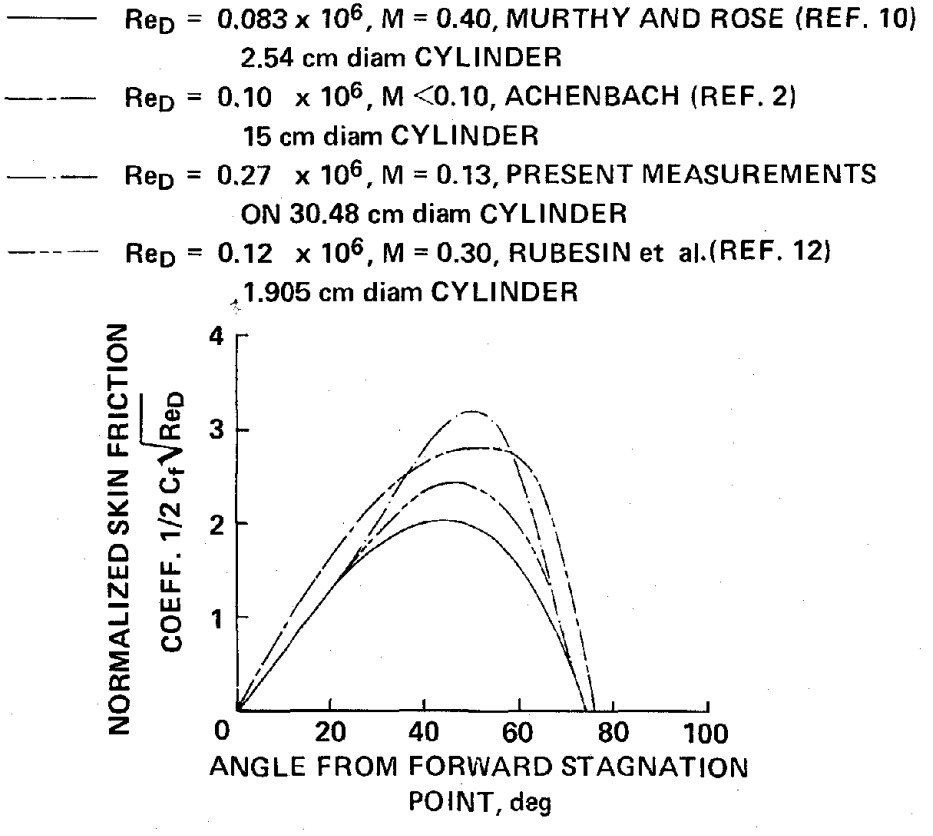
Re$_D$ = 0.083 x 10^6, M = 0.40, MURTHY AND ROSE (REF. 10)
2.54 cm diam CYLINDER
Re$_D$ = 0.10 x 10^6, M <0.10, ACHENBACH (REF. 2)
15 cm diam CYLINDER
Re$_D$ = 0.27 x 10^6, M = 0.13, PRESENT MEASUREMENTS
ON 30.48 cm diam CYLINDER
Re$_D$ = 0.12 x 10^6, M = 0.30, RUBESIN et al.(REF. 12)
1.905 cm diam CYLINDER
NORMALIZED SKIN FRICTION COEFF. 1/2 $C_f\sqrt{Re_D}$
4
3
2
1
0
20
40
60
80
100
ANGLE FROM FORWARD STAGNATION POINT, deg

Figure 10.- Skin friction distribution on circular cylinder.

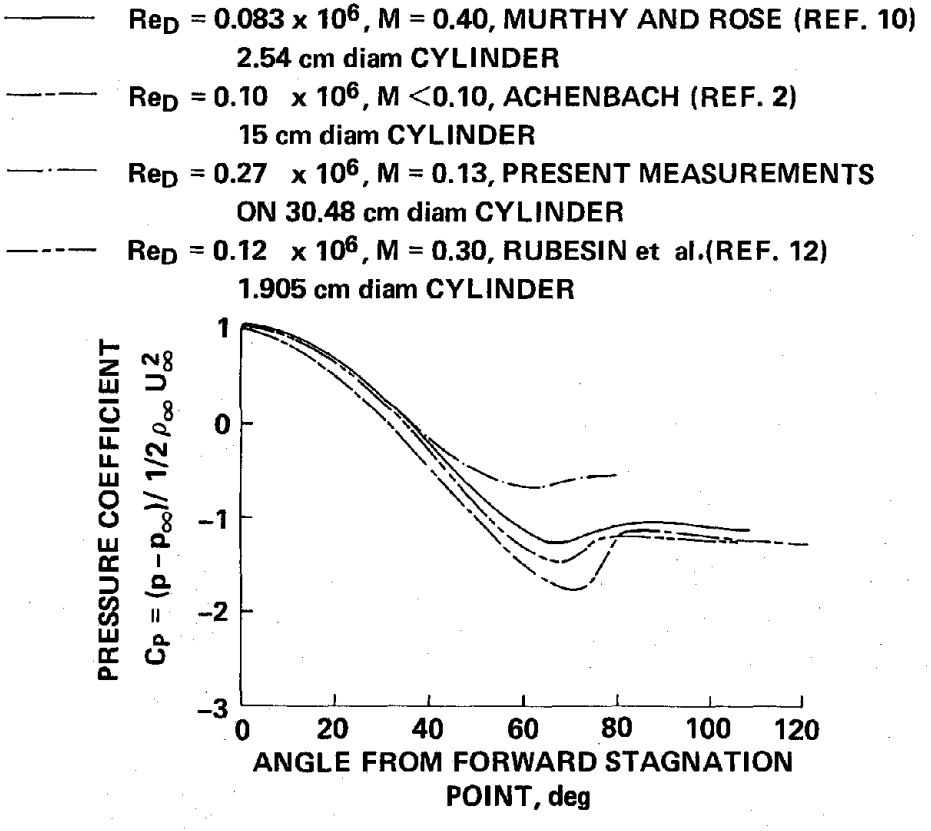

Figure 11.- Pressure distribution on circular cylinder.

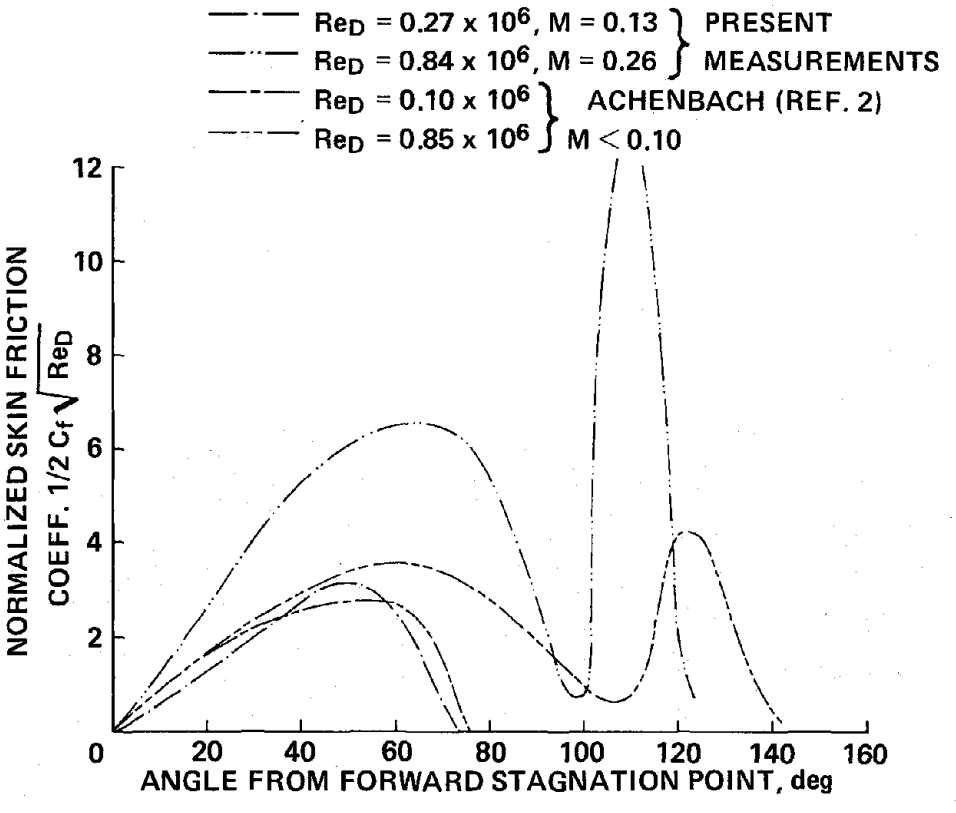

Figure 12.- Skin friction distribution on circular cylinder.

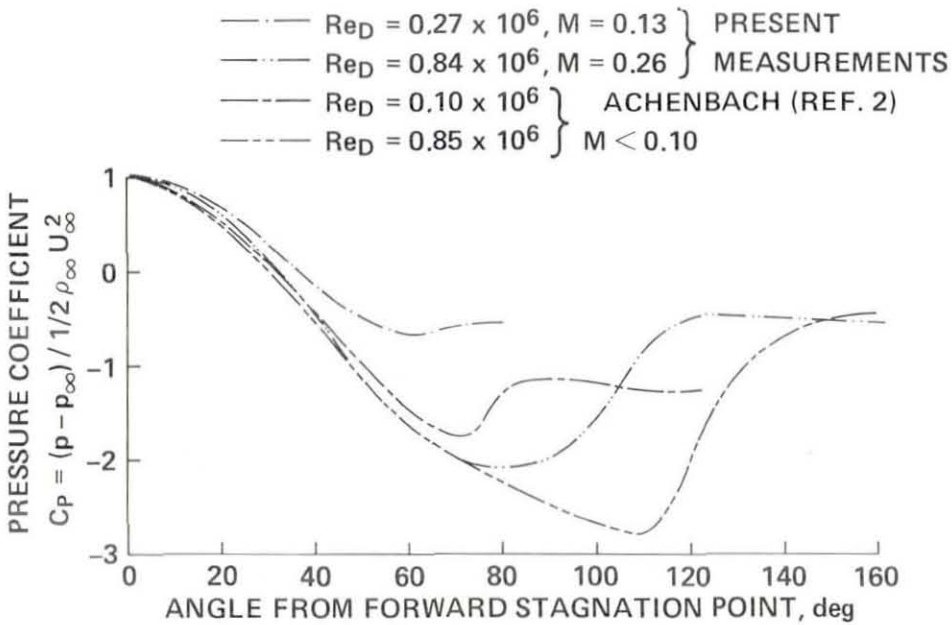

Figure 13.- Pressure distribution on circular cylinder.

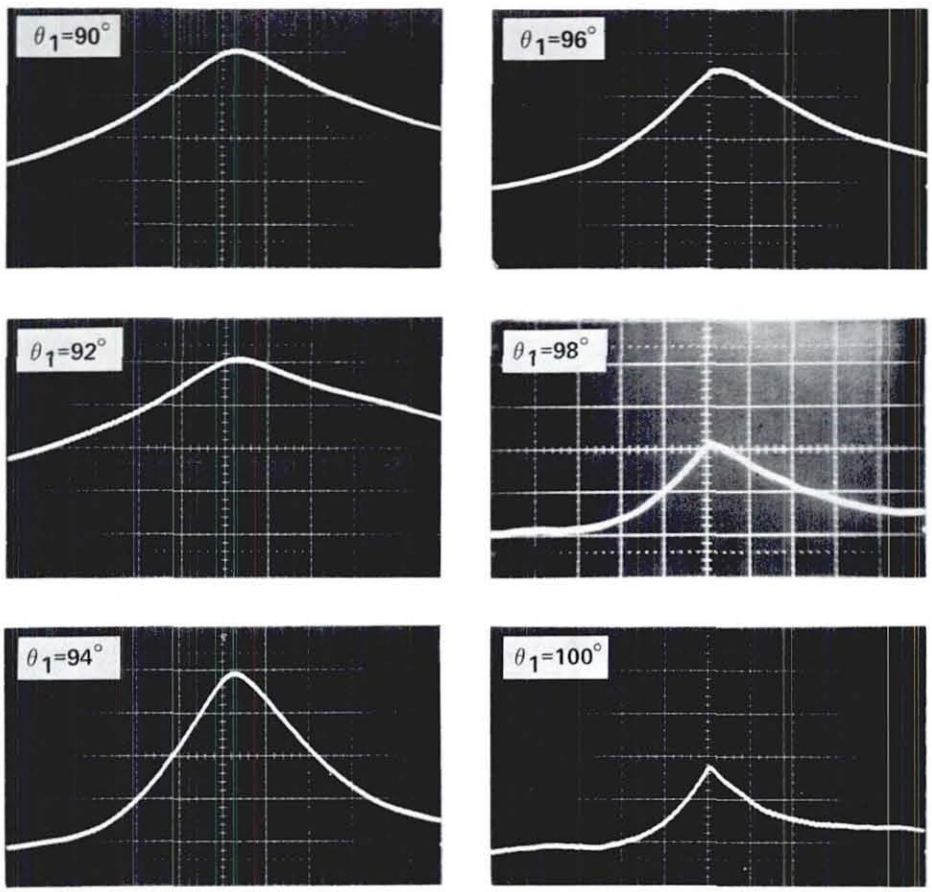

ORDINATE: $\sum_i V_1(t_i - \delta t) \cdot V_2(t_i)$

$V_{1,2}(t_i)$: GAGE OUTPUT VOLTAGE AT TIME t_i

ABCISSA : TIME DELAY (δt): 4 millisec/DIVISION
ZERO DELAY ADJUSTED TO MID-LINE

DELAY APPLIED TO FORWARD WIRE

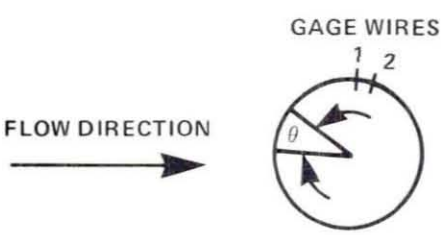

DISTANCE BETWEEN WIRES = 2.03 mm
CYLINDER DIAMETER = 304.8 mm
FREE-STREAM MACH NUMBER = 0.26
REYNOLDS NUMBER (based on diameter) = 7.0×10^6

Figure 14.- Cross correlation of adjacent gage wire signals across separation point for cross flow past circular cylinder, M = 0.26, $Re_D = 7.0 \times 10^6$.

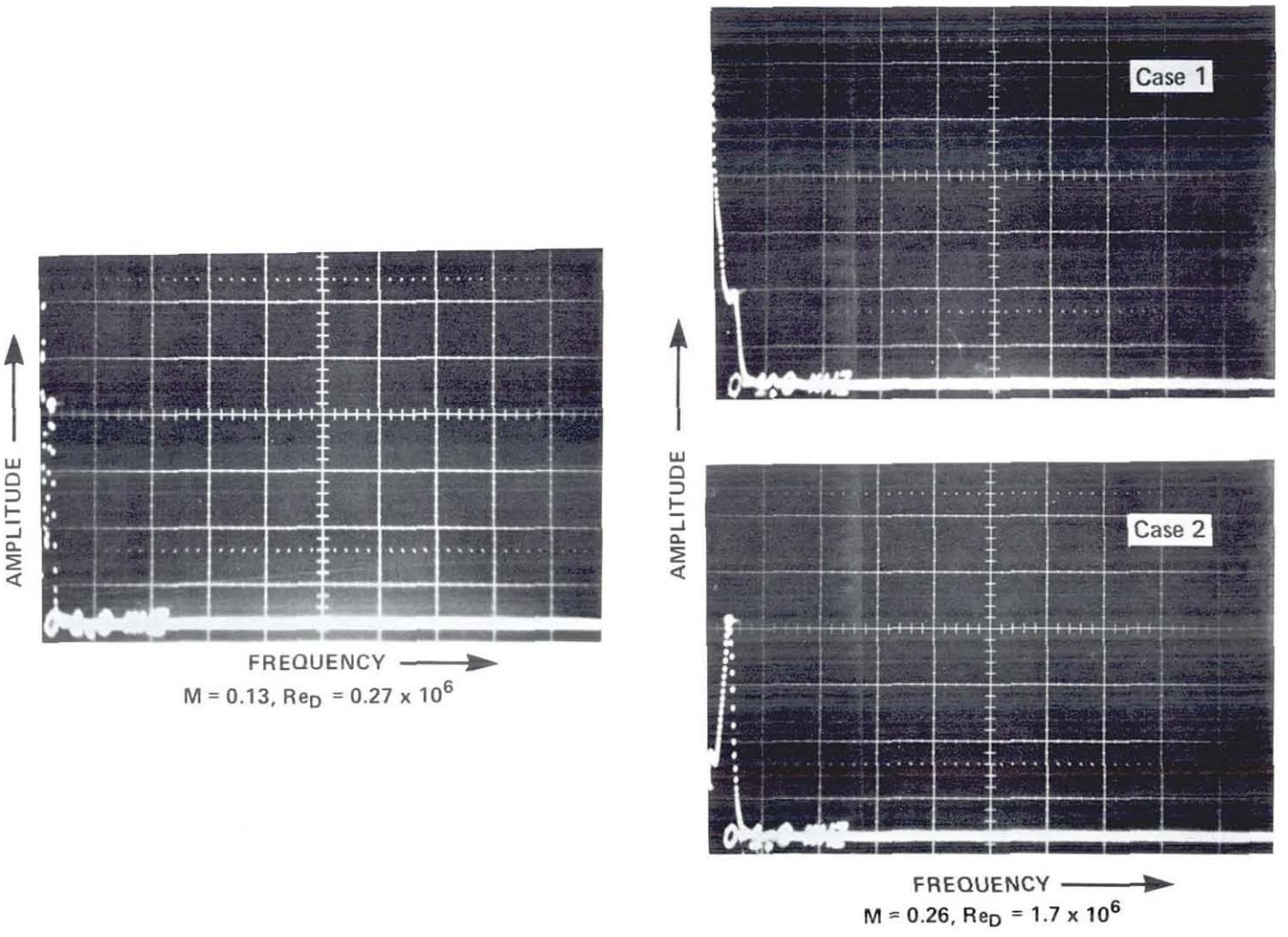

Figure 15.- Typical frequency spectrum of vortex shedding phenomenon for circular cylinders in cross flow.

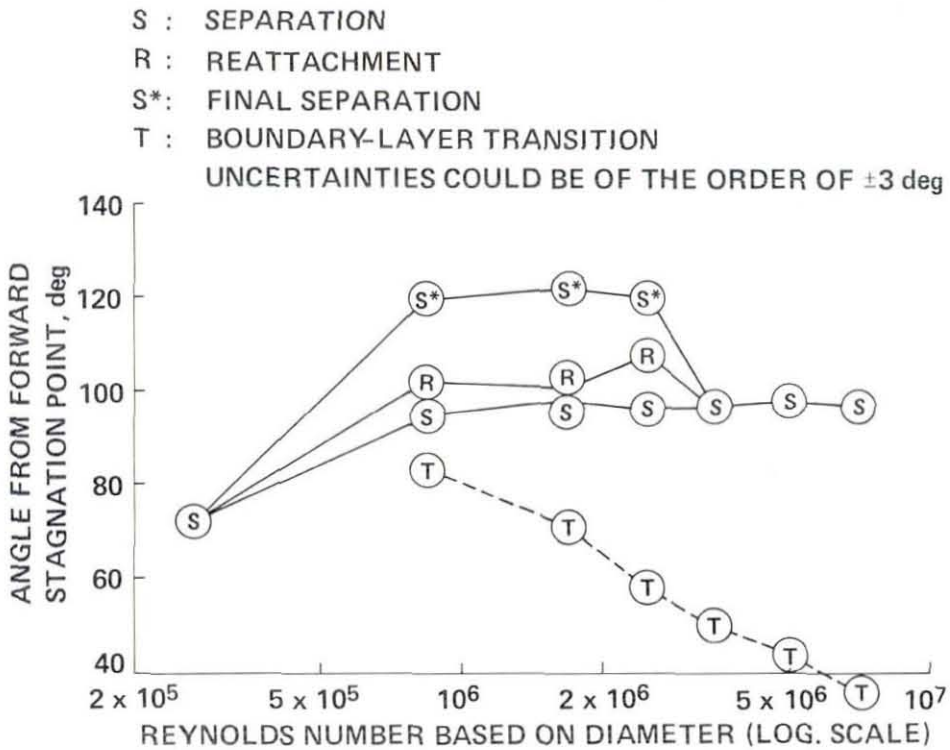

Figure 16.- Transition and separation phenomena for cross flow past circular cylinders.

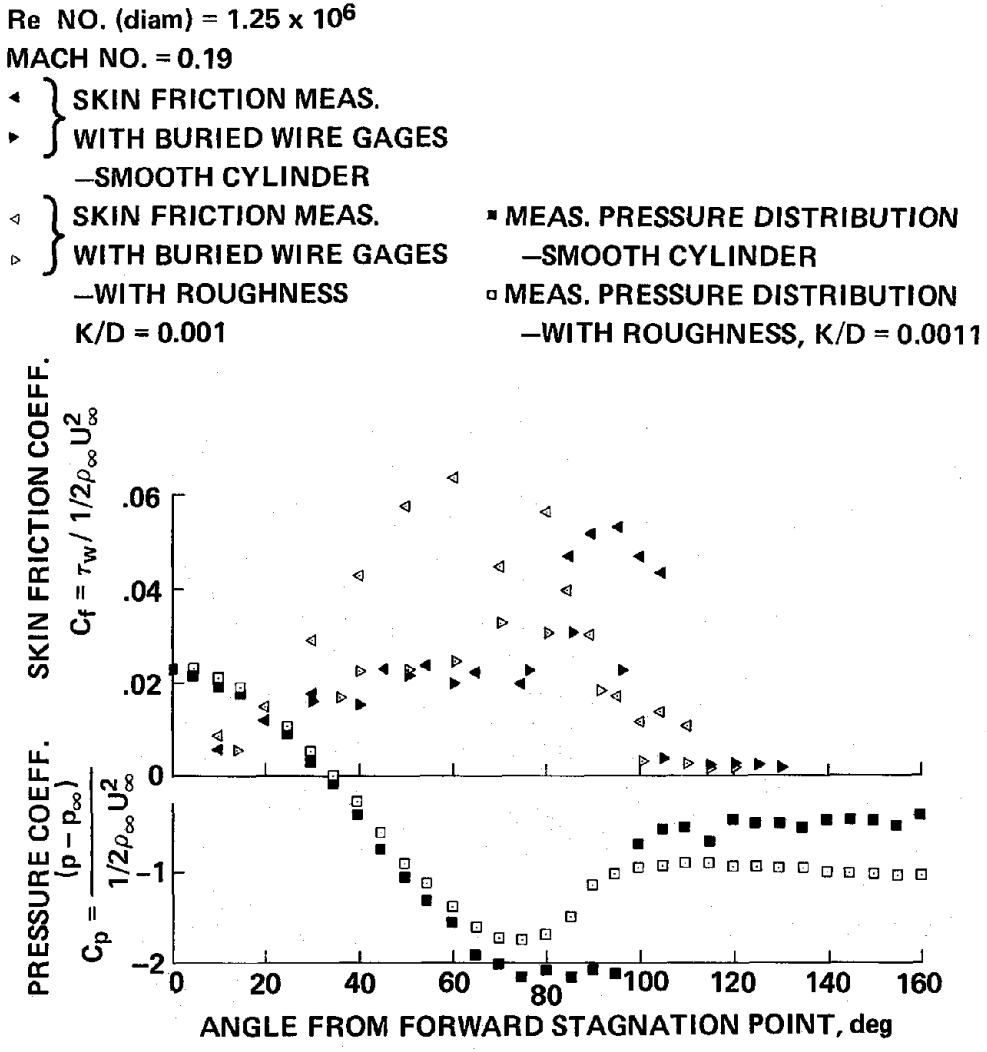

Figure 17.- Skin friction and pressure distributions on circular cylinder (with and without surface roughness).

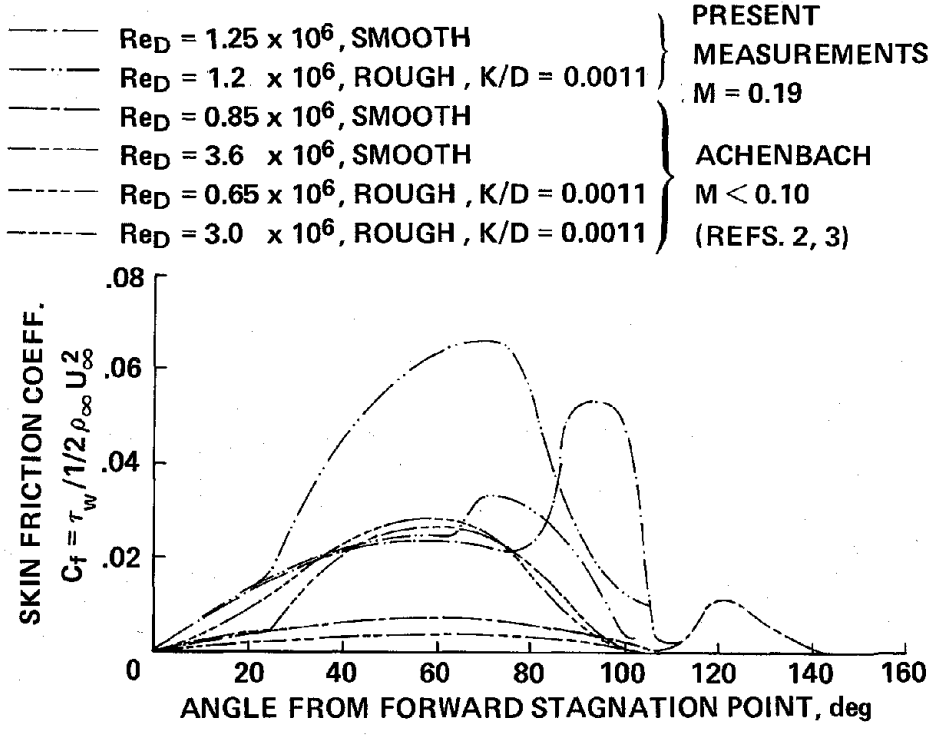

Figure 18.- Skin friction distribution on circular cylinder (with and without surface roughness).

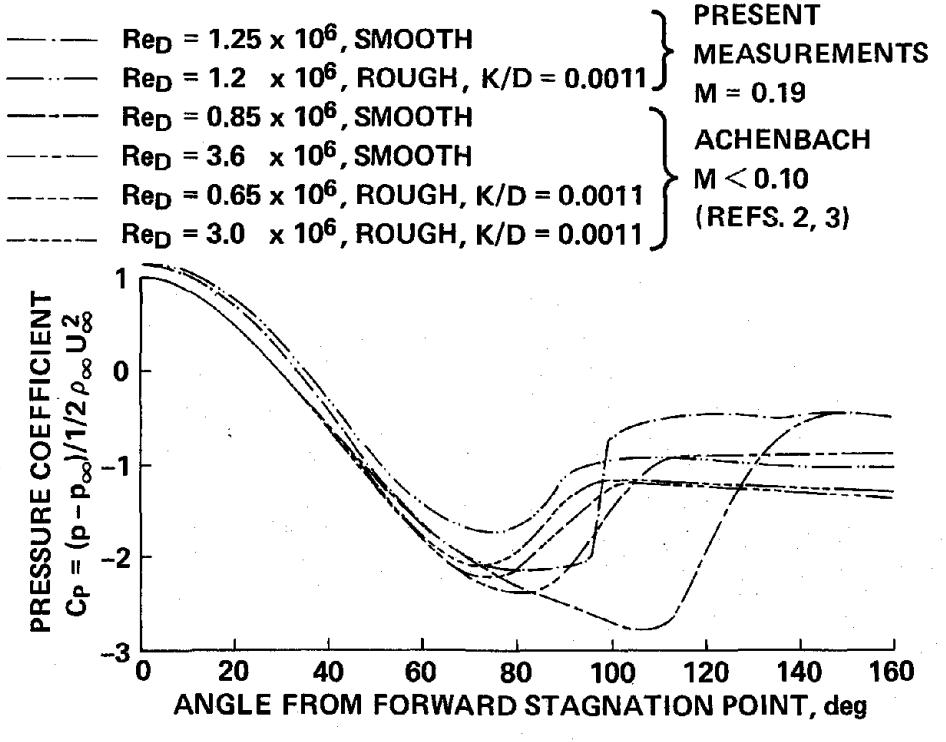

Figure 19.- Pressure distribution on circular cylinder (with and without surface roughness).